Dopamine gates prediction error forwarding in the cortices of the inferior colliculus

Catalina Valdés-Baizabal[1,2†], Guillermo V. Carbajal[1,2†], David Pérez-González[1,2*] & Manuel S. Malmierca[1,2,3*]

[1] Auditory Neuroscience Laboratory, Institute of Neuroscience of Castilla y León, Calle Pintor Fernando Gallego 1, 37007 Salamanca, Spain

[2] The Salamanca Institute for Biomedical Research (IBSAL), 37007 Salamanca, Spain.

[3] Department of Biology and Pathology, Faculty of Medicine, Campus Miguel de Unamuno, University of Salamanca, 37007 Salamanca, Spain

[†] Equal contribution

* Corresponding authors

Short title: Dopamine gates prediction error forwarding in the IC cortices

Keywords: inferior colliculus (IC), stimulus-specific adaptation (SSA), predictive coding, prediction error, precision, dopamine, auditory

Highlights

- Dopamine reduces the responsiveness of IC neurons to unexpected sounds exclusively.
- Dopamine decreases prediction error forwarding from the IC cortices.
- Dopaminergic input to the IC cortices encodes precision of prediction errors.

Abstract

Predictive coding theory describes perception as a hierarchical predictive model of sensation. Higher-level neural structures constrain the processing at lower-level structures by suppressing synaptic activity induced by predictable sensory input. But when predictions fail, deviant input is forwarded bottom-up as 'prediction error' to update the perceptual model. The earliest prediction error signals identified in the auditory pathway emerge from the cortices of the inferior colliculus (IC). The drive that each prediction error has on the perceptual model depends on its 'precision', which is theoretically encoded by the dopaminergic system. To test it empirically, we recorded single-unit responses from the rat IC cortices to oddball and cascade sequences before, during and after the microiontophoretic application of dopamine or eticlopride (a D_2-like receptor antagonist). Thereby, we studied dopaminergic modulation on the subcortical processing of unpredictable and predictable auditory changes. Results demonstrate that dopamine reduces neuronal responsiveness exclusively to unexpected auditory input. High dopamine concentrations in the neuronal microdomain reduce prediction error forwarding via D_2-like receptors, without significantly altering repetition suppression. Thus, already at subcortical levels of the auditory pathway, dopaminergic input to the IC gates the bottom-up flow of prediction error signals by encoding their precision.

List of abbreviatures

CAS: deviant condition.

CSI: common SSA index.

dB SPL: decibels sound pressure level.

DEV: deviant condition.

FRA: frequency response area.

IC: inferior colliculus.

iMM: index of neuronal mismatch.

iPE: index of prediction error.

iRS: index of repetition suppression.

mRNA: messenger RNA

PSTH: peristimulus time histogram.

SPF: subparafascicular nucleus of the thalamus.

SSA: stimulus-specific adaptation.

STD: standard condition.

TDT: Tucker-Davis Technologies.

Introduction

Perceptual systems prune redundant sensory input as a means of sparing processing resources while providing saliency to input that is rare, unique, and therefore potentially more informative. This perceptual function has been classically studied in humans using the auditory oddball paradigm (Fig. 1A) [1], where the successive repetition of a tone (‘standard condition’, henceforth ‘STD’) is randomly interrupted by an ‘oddball’ tone (‘deviant condition’, henceforth ‘DEV’). When applied to animal models, the oddball paradigm unveils a phenomenon of neuronal short-term plasticity called stimulus-specific adaptation (SSA), measured as the difference between DEV and STD responses [2].

SSA first emerges in the auditory system at the level of the inferior colliculus (IC) [3]. As a site of convergence of both ascending and descending auditory pathways, the IC plays a key role in processing deviant sounds over redundant ones [4] and shaping the auditory context [5]. The complex computational network of the IC integrates excitatory, inhibitory and rich neuromodulatory input [6,7], which includes dopaminergic innervation from the subparafascicular nucleus (SPF) of the thalamus [8–12]. Previous studies have revealed that other neuromodulators such as acetylcholine [13] and endocannabinoids [14] intervene in the regulation of SSA in the IC, but the involvement of dopamine-dependent mechanisms is yet to be confirmed.

A neurobiologically informed theory of predictive coding, known as hierarchical perceptual inference [15–17], posits that hierarchically coupled neuronal populations represent sensory regularities into a predictive perceptual model that explains predictable input away. Information about unexpected stimuli is encoded in the form of prediction error signals, transmitted ‘bottom-up’ through forward

connections as input for superior processing levels; whilst predictions about expected stimulus patterns are sent ‘top-down’ along backward connections, which constrain the processing performed at inferior levels. Neurons receiving top-down predictions decrease their responsiveness to expected sensory inputs, which during an oddball paradigm manifest functionally as *repetition suppression* of the STD response. But when encountering a DEV, the perceptual model fails to predict the ‘oddball’, so the unexpected sensory input will be forwarded as a *prediction error*.

According to this interpretation, the oddball paradigm induces two processes: (1) *repetition suppression* during STD, and (2) *prediction error* signaling during DEV [18]. A way to estimate the relative contribution of these two components to the total amount of SSA is to compare DEV and STD responses to those elicited by the cascade sequence (Fig. 1B) [19]. The predictable succession of ascending or descending frequencies generated by the ‘cascade condition’ (henceforth ‘CAS’) has proven to serve as an effective no-repetition control for the oddball paradigm (Fig. 1C), both in humans [20] and in animal models [21].

Prediction errors are not infallible, but the product of an inferential process. Therefore, perceptual systems implement mechanisms to adjust the relative influence of prediction error signals over perception. The weight of prediction errors on the perceptual model depends on their *precision*, formally defined as the inverse of their variance [22,23]. In neurobiological terms, predictive coding proposes that precision is encoded through neuromodulation, which regulates forward message-passing modulating the postsynaptic gain [24,25]. Furthermore, hierarchical inference models have particularly theorized about the

involvement of the dopaminergic system in encoding precision of prediction erros [26].

In this study, we perform microiontophretic injections of dopamine and eticlopride (a D_2-like receptor antagonist) while recording single-unit responses under DEV, STD and CAS conditions to determine whether dopaminergic input to the IC modulates predictive auditory processing. Our results demonstrate that dopamine has a profound effect on how unexpected sounds are processed in the IC cortices, probably by lowering the precision of prediction error signals.

Materials and Methods

Surgical procedures

We conducted experiments on 31 female Long-Evans rats aged 9–17 weeks with body weights between 150–250 gr. All methodological procedures were approved by the Bioethics Committee for Animal Care of the University of Salamanca (USAL-ID-195), and performed in compliance with the standards of the European Convention ETS 123, the European Union Directive 2010/63/EU and the Spanish Royal Decree 53/2013 for the use of animals in scientific research.

We first induced surgical anesthesia with a mixture of ketamine/xylazine (100 and 20 mg/Kg respectively, intramuscular) and then maintained it with urethane (1.9 g/Kg, intraperitoneal). To ensure a stable deep anesthetic level, we administered supplementary doses of urethane (~0.5 g/Kg, intraperitoneal) when the corneal or pedal withdrawal reflexes were present. We selected urethane over other anesthetic agents because it better preserves normal neural activity, having a modest, balanced effect on inhibitory and excitatory synapses [27–30].

We recorded auditory brainstem responses (ABR) with subcutaneous needle electrodes to verify the normal hearing of the rat. We acquired the ABR using a RZ6 Multi I/O Processor (Tucker-Davis Technologies, TDT) and immediately process it with BioSig software (TDT) before beginning each experiement. ABR stimuli consisted of 0.1 ms clicks at a rate of 21 clicks/s, delivered monaurally to the right ear in 10 dB steps, from 10 to 90 decibels of sound pressure level (dB SPL), in a closed system through a Beyer DT-770 earphone (0.1–45 kHz) fitted with a custom-made cone and coupled to a small tube (12 gauge hypodermic) sealed in the ear.

After normal hearing was confirmed, we placed the rat in a stereotaxic frame where the ear bars were replaced by hollow specula that accommodated a sound delivery system. We performed a craniotomy in the left parietal bone to expose the cerebral cortex overlying the left IC. We removed the dura overlying the left IC and covered the exposed cortex with 2% agar to prevent desiccation.

Data acquisition procedures

Experiments were performed inside a sound-insulated and electrically shielded chamber. All sound stimuli were generated using the RZ6 Multi I/O Processor (TDT) and custom software programmed with OpenEx Suite (TDT) and Matlab™ (Mathworks). In search of evoked auditory neuronal responses from the IC, we presented white noise bursts and sinusoidal pure tones of 75 ms duration with 5 ms rise-fall ramps. Once the activity of a single neuron was clearly isolated, we only used pure tones to record the experimental stimulation protocols. All protocols run at 4 stimulus per second and were delivered monaurally in a close-field condition to the ear contralateral to the left IC through

a speaker. We calibrated the speaker using a ¼-inch condenser microphone (model 4136, Brüel&Kjær) and a dynamic signal analyzer (Photon+, Brüel&Kjær) to ensure a flat spectrum up to ~73 dB SPL between 0.5 and 44 kHz, and that the second and third signal harmonics were at least 40 dB lower than the fundamental at the loudest output level.

To record extracellular single-unit activity while carrying out microiontophoretic injections, we attached a 5-barrel glass pipette to a hand-manufactured, glass-coated tungsten microelectrode (1.4–3.5 MΩ impedance at 1 kHz), with the tip of the electrode protruding 15-25 µm from the pipette tip [31]. One individual electrode was used to record one single neuron at a time. We place the electrode over the exposed cortex, forming an angle of 20° perpendicularly rostral to the coronal plane. Using a piezoelectric micromanipulator (Sensapex), we advanced the electrode while measuring the penetration depth until we could observe a strong spiking activity synchronized with the train of searching stimuli.

Analog signals were digitized with a RZ6 Multi I/O Processor, a RA16PA Medusa Preamplifier and a ZC16 headstage (TDT) at 12 kHz sampling rate and amplified 251×. Neurophysiological signals for multiunit activity were band-pass filtered between 0.5 and 4.5 kHz. Stimulus generation and neuronal response processing and visualization were controlled online with custom software created with the OpenEx suite (TDT) and MATLAB. A unilateral threshold for automatic action potential detection was manually set at about 2–3 standard deviations of the background noise. Spike waveforms were displayed on the screen and overlapped on each other in a pile-plot to facilitate isolation of single units. Only when all spike waveforms were identical and clearly separable form other smaller

units and the background noise, the recorded action potentials were considered to belong to a single unit.

Stimulation protocols

For all recorded neurons, we first computed the frequency-response area (FRA), which is the map of response magnitude for each frequency/intensity combination (Fig. 2). The stimulation procotol to obtain the FRA consisted of a randomized sequence of sinusoidal pure tones of 75 ms duration with 5 ms rise-fall ramps that was presented at a 4 Hz rate, randomly varying frequency and intensity of the presented tones (3–5 repetitions of all tones).

Protocol 1: Oddball paradigm (DEV and STD)

In a first round of experiments, we used the oddball paradigm (Fig. 1A) to study SSA. We presented trains of 400 stimuli containing two different frequencies (f_1 and f_2) presented in a pseudo-random order at a specific repetition rate (4 Hz) and at a level of 10–40 dB above threshold. Both frequencies were within the excitatory FRA previously determined for the neuron (Fig. 2). One frequency (f_1) appeared with high probability within the sequence (STD; P=0.9). The succession of STD tones was randomly interspersed with the second frequency (f_2), presented with low probability within the sequence (DEV; P=0.1). After obtaining one data set, the relative probabilities of the two stimuli were reversed, with f_2 becoming the STD and f_1 becoming the DEV. This allows to control for the physical characteristics of the sound in the evoked response, such that the differential response between DEV and STD of a given tone can only be due to their differential probability of appearance. Please beware that only the

last STD tone preceding each DEV was considered for the analysis (Fig. 1A, bottom panel), so we obtained 40 condition measurements per oddball paradigm played (Fig. 1A). We chose a 0.28 octave separation between frequencies in this round of experiments in order to allow result comparisons with previous SSA studies in the IC [3].

Protocol 2: Oddball paradigm (DEV and STD) + Cascade sequence (CAS)

In light of the recent discovery of prediction error signals recorded in IC neurons [21], we decided to adapt our stimulation protocol to that of Parras, Nieto-Diego and colleagues for a second round of experiments which incorporated the cascade sequence [19]. By arranging a bunch of tones in a regular succession of ascending or descending frequency, no tone is ever immediately repeated. In consequence, whereas CAS does not induce repetition suppression—as opposed to STD—, its pattern remains predictable, so the next tone in the sequence can be expected—as opposed to DEV—. Thus, CAS serves as control for the repetition effects elicited by STD, allowing SSA measurements to be dissociated in two components: *repetition suppression* and *prediction error* (Fig. 1C).

Therefore, after computing the FRA (Fig. 2), we selected 10 evenly-spaced tones at a fixed sound intensity 10–40 dB above minimal response threshold, so that at least two tones fell within the FRA limits. These 10 frequencies were separated from each other by 0.5 octaves, in order to make the results comparable to those of [21]. We used the 10 tones to build the ascending and descending versions of CAS (Fig. 1B). We selected 2 tones within that lot to

generate the ascending and descending versions of the oddball paradigm (Fig. 1A), comparing the resultant DEV with their corresponding CAS versions (Fig. 1B. All sequences were 400 tones in length, at the same, constant presentation rate of 4 Hz. Thus, each frequency could be compared with itself in DEV, STD and CAS conditions (Fig. 1C).

Dopaminergic manipulation procedures

After recording the chosen stimulation protocol in a *'control condition'*, i.e., before any dopaminergic manipulation, we applied dopamine or the D_2-like receptor antagonist eticlopride (Sigma-Aldrich Spain) iontophoretically through multi-barreled pipettes attached to the recording electrode. The glass pipette consisted of 5 barrels in an H configuration (World Precision Instruments, catalogue no. 5B120F-4) with the tip broken to a diameter of 30–40 µm [31]. The center barrel was filled with saline for current compensation (165 mM NaCl). The others were filled with dopamine (500 mM) or eticlopride (25 mM). Each drug was dissolved in distilled water and the acidity of the solution was adjusted with HCl to pH 3.5 for dopamine and pH 5 for eticlopride. The drugs were retained in the pipette with a -20 nA current and ejected using 90 nA currents (Neurophore BH-2 system, Harvard Apparatus). Thus, we released dopamine or eticlopride into the microdomain of the recorded neuron at concentrations that have been previously demonstrated effective in *in vivo* studies [10]. 5-15 minutes after the drug injection, we repeated the stimulation protocol during the *'drug condition'* until the drug was washed away. We considered the *'recovery condition'* when the spike count returned to levels that did not significantly differ from control values, never before 40 minutes post-injection.

We used both dopamine and eticlopride during protocol 1, while only dopamine was tested protocol 2. During protocol 1, in a few occasions where the recording was exceptionally stable, after the first recovery we performed a second injection using the other drug (Fig. 5A-B). This prolonged procedure was meant to test the consistency of dopaminergic effects (agonist versus antagonist) within individual neurons when possible.

Data analysis

All the data analyses were performed with SigmaPlot™ (Systat Software) and MATLAB software, using the built-in functions, the Statistics and Machine Learning toolbox for MATLAB, as well as custom scripts and functions developed in our laboratory. All average values in the present study are expressed as mean±SEM (standard error of the mean).

Peristimulus histograms (PSTH)

Taking the 40 trials available for each tone and condition, we computed a PSTH representing the action potential density over time in spikes per second from −75 to 250 ms around stimulus onset (Fig. 3E-F, 4E-F and 5A-B). We smoothed the PSTH with a 6 ms gaussian kernel ("ksdensity" function in MATLAB) in 1 ms steps to estimate the spike-density function over time, and the baseline spontaneous firing rate was determined as the average firing rate (in spikes/s) during the 75 ms preceding stimulus onset. The excitatory response was measured as the area below the spike-density function and above the baseline spontaneous firing rate, between 0 and 180 ms after stimulus onset. We refer to this measure as 'baseline-corrected spike count'.

Common SSA index (CSI)

For our 'classic' study of SSA, we used the Common SSA Index (CSI) [2], replicating the methodology of previous studies of SSA neuromodulation in the IC [13,14,32,33]. For the pair of frequencies in each oddball paradigm, the CSI was calculated as:

$$CSI = \frac{DEV_{f1} + DEV_{f2} - STD_{f1} - STD_{f2}}{DEV_{f1} + DEV_{f2} + STD_{f1} + STD_{f2}}$$

Where DEV_{fi} and STD_{fi} are spike counts in response to a frequency f_i when it was presented in deviant and standard conditions, respectively. The CSI ranges between -1 to +1, being positive if the response to the deviant condition was greater than the standard condition.

Indices of neuronal mismatch (iMM), repetition suppression (iRS) and prediction error (iPE)

We analyzed protocol 2 results replicating the methodology of a previous study which pioneered the use of the cascade sequence to control for the repetition effects of the oddball paradigm in IC neurons (see [21] for a more exhaustive report on the analysis). The rationale was that, whereas the physical conditions of the auditory change are the same during the oddball and cascade sequences (i.e., an ascending or descending step of 0.5 octaves), the predictions generated by the perceptual model were different in DEV and CAS. Therefore, a different neuronal response to DEV and CAS could only be do the fact that DEV violates a prediction of the perceptual model whereas CAS fulfills it.

During the oddball paradigm, the STD is highly predictable and swiftly fits into a perceptual model of the repetition that organizes the auditory sequence. Hence, the predictions of the perceptual model will induce a strong repetition

suppression on the elicited response to that tone when presented as STD. Conversely, when that same tone is presented as a DEV, its occurrence is completely unpredictable and will not fit into the repetition rule encoded in the internal model of the stimulation. Consequently, the internal model will signal a prediction error in response to DEV.

During CAS, on the other hand, the target tone f_i will be immersed within a regular succession of ascending or descending frequencies. This arrangement is predictable without featuring the repetition rule that organizes the train of tones in the STD. Therefore, the difference between the CAS and the STD response must be due to repetition suppression. Once repetition suppression has been accounted for, we considered the remaining response in SSA (whether present) as an extra component that could only correspond to prediction error signaling [18]. The cascade sequence thereby allows to dissociate SSA in 2 components: repetition suppression and prediction error (Fig. 1C).

Thus, we used the cascade sequence to control for the repetition effects induced by the oddball paradigm (for extended rationale, see [18,19]) and decompose SSA into *prediction error* and *repetition suppression* components. To allow comparison between responses from different neurons, we normalized the spike count evoked by each tone in DEV, STD and CAS as follows:

$$DEV_N = \frac{DEV}{N} \;\; ; \;\; STD_N = \frac{STD}{N} \;\; ; \;\; CAS_N = \frac{CAS}{N}$$

Where,

$$N = \sqrt{DEV^2 + STD^2 + CAS^2}$$

From these normalized responses, we computed the indices of *neuronal mismatch* (iMM), *repetition suppression* (iRS) and *prediction error* (iPE) as:

$$iMM = DEV_N - STD_N$$

$$iRS = CAS_N - STD_N$$

$$iPE = DEV_N - CAS_N$$

These indices range between -1 and 1. The iMM is largely equivalent to the classic CSI as an index of SSA, as previously demonstrated by Parras, Nieto-Diego and colleagues [21], see Supplementary Figure 2). Nevertheless, please beware the CSI provides one index for each pair of tones in the oddball paradigm, whereas the iMM provides one index for each tone tested (the same as the iPE and the iRS).

Dopaminergic effects analysis

We followed the same procedure to analyze the results of stimulation protocols 1 and 2. First, we performed a Wilcoxon signed rank test using the *signrank* MATLAB function to compare all indices (CSI, iMM, iRS and iPE) under control versus drug conditions for the whole population of neurons.

Then, we performed a bootstrapping to analyze dopaminergic effects on each individual neuron. SSA indices, both CSI [2] and iMM [21], are statistics resulting from a complex combination of the single-trial responses to DEV, STD and CAS. In consequence, the sample distribution of those indices for any neuron is highly non-normal, and confidence intervals of such sample cannot be easily determined using analytical methods. Therefore, to test the drug effects on each individual neuron, we calculated the 95% bootstrap confidence intervals for the baseline SSA index using the *bootci* MATLAB function with 1000 bootstrap samples, as in previous studies of SSA neuromodulation in the IC [13,14,32,33]. We considered drug effects to be significant when the confidence intervals of the

SSA indices under control and drug conditions did not overlap. We analyzed those neurons that showed significant SSA index changes due to dopaminergic manipulation using the Wilcoxon signed rank test.

Finally, we performed a linear regression between the changes observed in the iMM and those observed in the iRS and iPE using the MATLAB function *fitlm*. Index changes were calculated as:

$$iMM_{change} = iMM_{dopamine} - iMM_{control}$$

$$iPE_{change} = iPE_{dopamine} - iPE_{control}$$

$$iRS_{change} = iPE_{dopamine} - iPE_{control}$$

Histological verification procedures

At the end of each experiment, we inflicted electrolytic lesions (5 μA, 5 s) through the recording electrode. Animals were sacrificed with a lethal dose of pentobarbital, after which they were decapitated, and the brains immediately immersed in a mixture of 1% paraformaldehyde and 1% glutaraldehyde in 1 M PBS. After fixation, tissue was cryoprotected in 30% sucrose and sectioned in the coronal plane at 40 μm thickness on a freezing microtome. We stained slices with 0.1% cresyl violet to facilitate identification of cytoarchitectural boundaries. Finally, we assigned the recorded units to one of the main subdivisions of the IC using the standard sections from a rat brain atlas as reference [34].

Results

In order to study the role of dopamine in shaping SSA in the IC, we recorded responses from a total of 196 well-isolated neurons in 31 young adult Long Evans rats. In a first series of experiments (protocol 1, see methods) we

recorded from 142 single units using the oddball paradigm before, during and after microiontophoretic application of dopamine (n=94), eticlopride (n=43) or both drugs, one after the other (n=5). In an additional series of experiments (protocol 2, see methods), we recorded from 54 single units before, during and after microiontophoretic application of dopamine, this time presenting two cascade sequences (ascending and descending) in addition to the oddball paradigm [21]. Histological verification located all recorded neurons in the cortices of the IC, where SSA indexes are higher [3,4].

Dopamine effects on the CSI

The microiontophoretic application of dopamine during protocol 1 caused an average SSA decrease of -16% in our sample, falling from a control CSI of 0.51±0.03 to 0.43±0.04 after dopamine application ($p=0.007$). Such reduction was caused by a -30% drop in the average DEV response ($p<0.001$), while STD response tended to remain stable ($p=0.913$).

We performed a bootstrap analysis to evaluate the statistical significance of the effect of dopamine on each individual neuron. Depending on the neuron, dopamine caused the CSI to either increase, decrease or remain stable showing no significant change. These heterogeneous effects were visible in the FRA (Fig. 2). Thus, we separated the population into 3 different groups. In one group, CSI decreased significantly after dopamine application (n=39; Fig 3A, purple circles below the diagonal), while in a second group, the CSI increased significantly (n=30; Fig 3A, purple circles above the diagonal). Both groups showed CSI changes above 50% on average (Fig 3B). In a third group of neurons, CSI did not

change significantly (n=25; Fig 3A, grey dots); these neurons were excluded from further analyses, since they were not affected by dopamine.

We also analyzed the firing rate of the neurons where dopamine caused a significant CSI change. For the group of neurons where the CSI decreased (n=39), the firing rate increased significantly in response to STD (30%; p=0.009), whereas no significant changes appeared in the DEV response (p=0.114; Fig 3C). Besides, the spontaneous firing rate increased (61%; p<0.001) in this group of neurons. In contrast, in the group of neurons where the CSI increased (n = 30), the firing rate decreased significantly in response to both STD (-61%; p < 0.001) and DEV (-38%; p = 0.002; Fig 3D), as well as the spontaneous firing rate (-50%; p < 0.001). No significant changes were observed in the average first spike latency of any group or condition.

Examples of neurons within these two groups are displayed in Figure 3E-F. Figure 3E shows the response of a neuron to STD (blue) and DEV (red) in the control condition (left panel), during dopamine application (middle panel) and after recovery (right panel). The application of dopamine caused an increment of the STD response and a decrement of the DEV response, leading to a decrease of the CSI. In contrast, the example in Figure 3F showed a decrement of the response to both STD and DEV during the application of dopamine, thus resulting in an increase of the CSI. The effects of dopamine peaked around 8-10 minutes after microiontophoretic application, followed by a progressive recovery of the responses to baseline values that could take beyond 90 minutes (Fig. 3E-F, right panels).

Eticlopride effects on the CSI

To test whether SSA was modulated through D_2-like receptors, we recorded 43 neurons under the influence of eticlopride, a dopamine D_2-like receptor antagonist. We observed a subtle increase of the average CSI from 0.26±0.04 to 0.29±0.04 after eticlopride application that failed to reach statistical significance (p=0.234).

Eticlopride produced diverse effects depending on the neuron, as it was the case for dopamine application (Fig. 4E-F). Accordingly, we performed the same bootstrap analysis to separate the neurons into 3 groups, depending on the presence and direction of significant changes. Eticlopride increased the CSI in 15 units (Fig 4A, green circles above the diagonal) and decreased the CSI in 8 units (Fig 4A, green circles below the diagonal). These two subgroups did not show any significant changes in their DEV and STD responses. Nonetheless, in the group of neurons where the CSI decreased, the DEV firing rate tended to decrease and the STD firing rate tended to increase, while opposite effects where found for the group of neurons where the CSI increased (Fig. 4C-D). Examples from these two subgroups are displayed in Figure 4E-F. The remaining 20 units underwent non-significant CSI changes after eticlopride application (Fig 4A, grey circles).

Application of dopamine and eticlopride on the same neuron

We aimed to determine whether dopaminergic effects in the IC were mediated by D_2-like receptors, as suggested in previous reports [9,35]. To do this, we took advantage of 5 single-units exceptionally stable during the recording session to test whether dopamine and eticlopride had consistently opposite

effects in each one. We recorded the activity of these 5 neurons in control conditions, and then during an application of either dopamine or eticlopride. After enough time had passed for the neurons to recover from the effects of the first drug (never less than 40 minutes post-injection), we recorded their activity again and then applied the other drug. We recorded the neuronal activity under the effect of the second drug, after which we let the neuron recover and performed a final recording (Fig. 5A-B). In 4 of the 5 cases, dopamine was applied first and eticlopride second, and viceversa in the other case left.

Our results revealed that the dopaminergic effects were specifically mediated by D2-like receptors, as dopamine and eticlopride (D2-like receptor antagonist) induced complementary effects in each neuron tested (Fig. 5). Figure 5A and B show two single units illustrating the effect of a dopamine injection (time after first injection: ~5-15 mins), followed by its recovery (~40-65 mins) and a subsequent eticlopride injection (~65-80 mins) with its recovery (~120-140 mins). The CSI of the neuron displayed in Figure 5A decreases with the dopamine injection and increases with eticlopride. Conversely, yet consistently, the neuron illustrated in Figure 5B shows the opposite effects, increasing its CSI during the dopamine application and decreasing with eticlopride application. The bar plots in Figure 5C show the averaged effect of dopamine and eticlopride on various parameters, such as CSI, firing rate and first spike latency (for both DEV and STD) and spontaneous firing rate. All the parameters but one (DEV first spike latency) changed in opposite directions depending on the application of dopamine or eticlopride.

Dopamine effects on the iMM, the iPE and the iRS

To test whether dopamine modulates prediction error signaling in the IC cortices, we performed an additional set of experiments following stimulation protocol 2 (see methods), which was based on the methodology of a previous study [21]. Alongside the oddball paradigm, we recorded responses of 54 neurons to two cascade sequences (ascending and descending), which consisted of 10 tones selected within the FRA presented in a predictable succession of increasing or decreasing frequencies.

After normalizing the neuronal responses (see methods), we calculated the iMM, the iPE and the iRS for the whole population of neurons. Results agreed with those previously obtained using the CSI, as control iMM fell from 0.53±0.02 to 0.43±0.03 under dopaminergic influence (p=0.003; Fig. 6B, all dots), representing a -19% drop on the population SSA. The median iPE for the whole population of neurons went down as well, from 0.05±0.03 to -0.06±0.04 after dopamine injection (p = 0.003; Fig. 6B, all dots). Conversely, the median iRS did not undergo any significant changes (from 0.48±0.03 to 0.50±0.03; p = 0.253; Fig. 6B, all dots). These results suggest that dopamine caused the average SSA index to reduce due to a decay in prediction error signaling.

As we did for the CSI, we used a bootstrap analysis to evaluate the statistical significance of the effect of dopamine on the iMM of each individual neuron. Similarly to the CSI, dopamine caused the iMM to either increase, decrease or remain stable depending on the neuron. We further analyzed how the response to each stimulus condition (DEV, STD and CAS) changed for those neurons which showed a significant change in their iMM induced by dopamine application. Whereas dopamine altered responses to neither CAS (p=0.052) nor

STD (p=0.094), the DEV responses underwent a -21% decrease (p=0.004; Fig. 6A). In consequence, dopamine-sensitive SSA neurons saw their iMM fall (from 0.57±0.02 in control to 0.36±0.03 under dopamine; p = 0.004; Fig. 6B, colored dots) along with their iPE (from 0.05±0.03 in control to -0.18±0.03 under dopamine; p = 0.008; Fig. 6C, colored dots) with the microiontophoretic application of dopamine, whereas individual changes in their iRS did not describe any significant tendency (from 0.52±0.03 in control to 0.53±0.03 under dopamine; p = 0.626; Fig. 6B, colored dots).

To evidence that this dopamine-induced decrease on SSA was due to diminished prediction error activity that could not be explained by changes in repetition suppression, we performed a regression model between changes in the iMM with changes in the iPE and the iRS (Fig. 7). A linear polynomial model unveiled a direct relationship between iMM and iPE changes, while no apparent relationship existed between iMM and iRS changes. Results were similar whether we consider the whole sample or just the dopamine-sensitive neurons.

The model for the whole sample of neurons (Fig. 7, all dots, gray line) was:

$$iPE_{change} = -0.01 + 1.09\left(iMM_{change}\right) ; R^2 = 0.48 ; p < 0.001$$

$$iRS_{change} = 0.01 - 0.09\left(iMM_{change}\right) ; R^2 = 0.01 ; p = 0.387$$

The model taking exclusively into account those neurons that individually manifested a significant iMM change induced by dopamine application (Fig. 7, colored dots and line) was:

$$iPE_{change} = -0.04 + 0.85\left(iMM_{change}\right) ; R^2 = 0.46 ; p < 0.001$$

$$iRS_{change} = 0.04 + 0.15\left(iMM_{change}\right) ; R^2 = 0.03 ; p = 0.363$$

Discussion

We recorded single-unit activity of neurons from the IC cortices under an auditory oddball paradigm while performing microiontophoretic applications of dopamine and eticlopride (D_2-like receptor antagonist) to investigate the role that the dopaminergic system plays in the processing of unexpected auditory events. Besides the oddball paradigm, we included cascade sequences to control for repetition suppression and thereby better assess dopaminergic effects on prediction error. Our results suggest that dopamine gates prediction error signals in the cortices of the IC.

Previous reports detected mRNA coding to D_2-like receptors in the IC [9,35] and proved its functional expression as protein [36]. Others studies demonstrated that dopamine modulates the auditory responses of IC neurons, yielding heterogeneous effects [10,36]. Here, we further confirm a functional expression of D_2-like receptors in neurons from the IC cortices and, for the first time, we describe the dopaminergic influence mediated by D_2-like receptors on the subcortical processing of unexpected auditory events.

Dopamine modulates SSA via D_2-like receptors

On average, dopamine application caused a 16-19% general reduction of SSA (measured as CSI and as iMM) in both of our neuronal samples from the IC cortices (Figs. 3A, 6B). Such SSA drop was brought about by a consistent decrease of DEV responses (Figs. 3C-D, 4C-D, 6A). The changes observed in the response of some neurons when eticlopride blockaded D_2-like receptors suggest that dopamine is being released endogenously in response to the sound, and that dopamine indeed plays a role at this early stage of auditory processing.

Most neurons in the IC cortices underwent significant individual changes and displayed heterogeneous sensitivities to dopaminergic manipulation (Fig. 3, 4). Most interestingly, the effects of dopamine and eticlopride were antagonistic within each individual neuron, such that whether the activation of D_2-like receptors by dopamine application increased the CSI, their blockade with eticlopride decreased the CSI (Fig. 5A), and viceversa (Fig. 5B). This tended to be the case also for the spontaneous activity, firing rate and first spike latency (Fig. 5C). We therefore conclude that those dopaminergic effects are mediated by D_2-like receptors expressed in the IC cortices. But probably not in the whole neuronal population of the IC cortices, since ¼ of our sample remained unaltered by dopaminergic manipulation (Fig. 3A, 4A, grey circles).

Characteristic synaptic properties may explain why dopaminergic manipulation generates divergent effects on each neuron. Both glutamatergic and GABAergic projections converge onto single IC neurons [6,37,38], which in the IC cortices may also receive dopaminergic inputs from the SPF [8–12]. Hence, dopaminergic manipulation could alter the balance of excitatory and inhibitory input of distinct neuronal types, as observed in other nuclei [39–42], consequently affecting their SSA in different manners. Thus, dopaminergic modulation in the IC cortices seems to rely heavily upon the characteristic synaptic properties of each neuron.

Dopamine encodes precision of prediction errors in the IC cortices

Since dopamine injections mainly reduced the neuronal responsiveness to DEV, we tested whether dopamine affected the processing of any auditory change (even if predictable) or it exclusively affected the processing of

unexpected auditory events. Therefore, together with the oddball paradigm, we implemented the cascade sequence [19] in a subset of experiments. The CAS allows to assess which proportions of SSA (measured as iMM) can be attributed to *repetition suppression* of the STD response (measured as iRS) or to pure *prediction error* signaling activity (measured as iPE) if any [18]. Thereby we could determine how these two functional components were differentially affected by dopamine. We found that most of the contrast between DEV and STD responses from IC neurons could be accounted for by repetition suppression. Yet, in many neurons, a significantly component of pure prediction error also contributed to the iMM, confirming previous observations [21].

In this sample, we found that dopamine application substantially diminished neuronal responsivity to DEV (-21%) while not affecting significantly neither STD nor CAS responses (Fig. 6A). This results in a decrease of the average iPE (Fig. 6C), whereas the iRS remained unaltered (Fig. 6D). Furthermore, our data revealed a clear direct relationship between the dopamine-induced iMM changes and the changes in the iPE (Fig. 7A), which did not exist for changes in the iRS (Fig. 7B). Thus, we conclude that dopaminergic input in the IC cortices is exclusively modulating the prediction error signals, i.e., the neuronal activity elicited by unexpected auditory events.

According to the hierarchical inference theory of predictive coding [15], perceptual systems represent the reliability of a sensory signal as *precision*, estimated as the inverse of its variance. Synaptic messages passed along the processing hierarchy are weighted by their precision, which regulates their integration into the perceptual model. When a synaptic input is granted high precision, the postsynaptic modulation exerts an amplifying effect on the output

error signal. Thus, reliable prediction errors will better drive the perceptual model. Conversely, when synaptic input describes extreme and random fluctuations, i.e., when sensory evidence is too ambiguous or noisy, a negative postsynaptic gain lessens the impact of those unreliable prediction errors on perception. Predictive coding literature regards neuromodulation as the biological embodiment of this precision-weighting mechanism [22,23,43]. Furthermore, many authors posit that the dopaminergic system reports reward prediction errors and encodes precision in contexts of uncertainty [26,44–47].

According to our data, dopamine may participate in precision encoding in the subcortical auditory pathway as well (Figs. 6, 7). Dopamine release in the cortices of the IC seems to associate prediction errors with a low precision, applying a negative gain that dampens the forward propagation of prediction error signals. Therefore, the concentration of dopamine in the IC cortices could be gating the bottom-up flow of prediction error, deeming their ‘reliability’ already at this early stage of auditory processing.

In natural conditions, such midbrain-level gating of prediction errors could be shaped by SPF dopaminergic neurons projecting to the cortices of the IC [11,35,48]. Many auditory nuclei project to the SPF, including auditory cortex, auditory thalamus, the IC and the superior olivary complex, providing it with rich auditory information [48–52]. Even other centers that perform higher-order functions in the perceptual processing and integration of auditory information send projections to the SPF, such as the medial prefrontal cortex and the deep layers of the superior colliculus [51]. Thus, the dopaminergic activity of the SPF must be interwoven to a great extend with the general functioning of the auditory system. The reciprocal connectivity of the SPF with many nuclei at multiple levels

of the auditory pathway could provide the structural basis for an optimal encoding of precision, modulating via dopaminergic input the weight of prediction errors forwarded from the IC cortices. This dopaminergic neuromodulatory network would allow the auditory system to manage the integration of meaningful and reliable sensory evidence from a very early stage of processing, indicating the fundamental implication of the IC in hierarchical perceptual inference.

Conclusions

The present study demonstrates that dopamine modulates perceptual processing of unexpected auditory events via D_2-like receptors. Our data reveal that dopamine down-regulates prediction error forwarding from the IC cortices, while leaving the effects repetition suppression relatively untouched. We propose that dopamine released in the cortices of the IC encodes the low precision of deviant-evoked synaptic activity, consequently reducing the postsynaptic gain of prediction error signals. This interpretation confers a gating function upon the IC cortices, which modulate the bottom-up flow of prediction errors based on the precision encoded through dopaminergic projections from the SPF. Thus, despite being usually neglected in the fundamentally cortical models of predictive coding, our study reinforces subcortical processing as a key element of hierarchical perceptual inference, at least in the auditory system.

Acknowledgments

CVB and GVC contributed equally to this work. We thank Drs Edward L Bartlett, Nell Cant, Adrian Rees and Richard Rosch for their useful comments on previous

versions of the manuscript. We also thank Mr Antonio Rivas Cornejo for taking care of histological processing.

Financial disclosure

Financial support provided by Spanish MINECO (SAF2016-75803-P) to MSM. CVB held a grant from Mexican CONACYT (216652). GVC held a fellowship from the Spanish MICINN (BES-2017-080030).

FIGURES

Figure 1

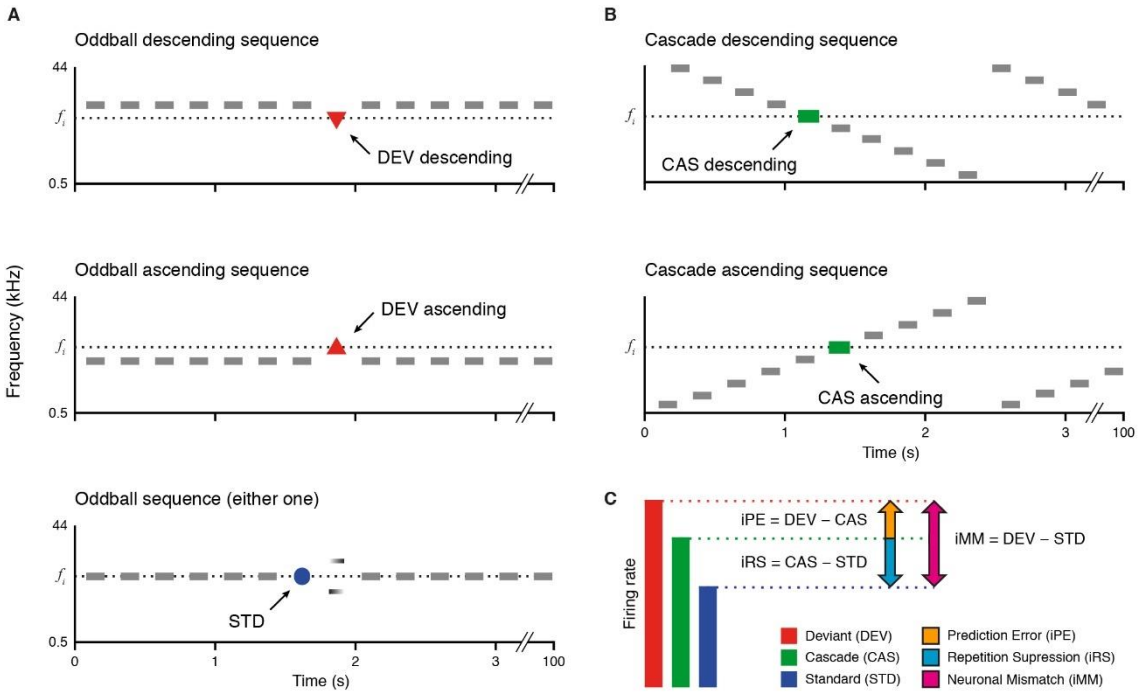

Figure 1. Stimulation protocols and interpretation. **A)** Oddball paradigm, displaying three possible experimental conditions for a given f_i target tone. **B)** Cascade sequences highlighting the f_i target tone, which is embedded in a predictable succession of equiprobable tones, allowing the system to establish a predictive rule that is not broken by the appearance of the target tone (as opposed

to DEV). CAS conditions are compared with the corresponding ascending or descending DEV. **C)** Dissociation of SSA in repetition suppression and prediction error indices.

Figure 2

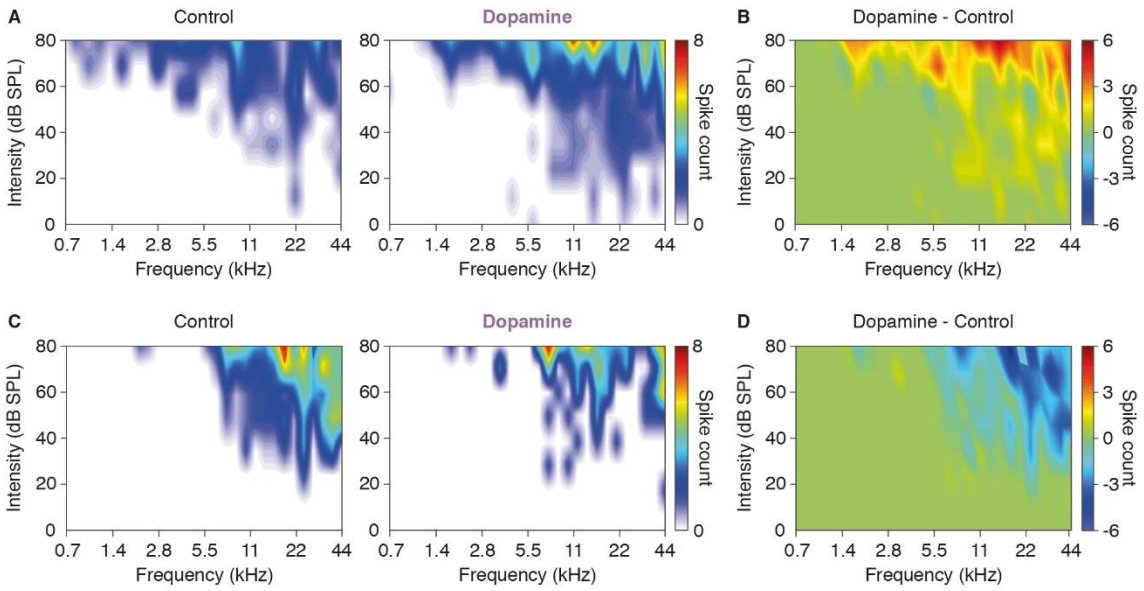

Figure 2. Effect of dopamine on the FRA. **A)** FRA of a neuron in control condition (left panel) and after dopamine application (right panel). **B)** The subtraction of the control FRA from that during application of dopamine in A reveals that dopamine increased the excitability of this neuron. **C)** FRA of another neuron in control condition (left panel) and after dopamine application (right panel). **D)** The subtraction of the control FRA from that during application of dopamine in C reveals that dopamine decreased the excitability of this neuron.

Figure 3

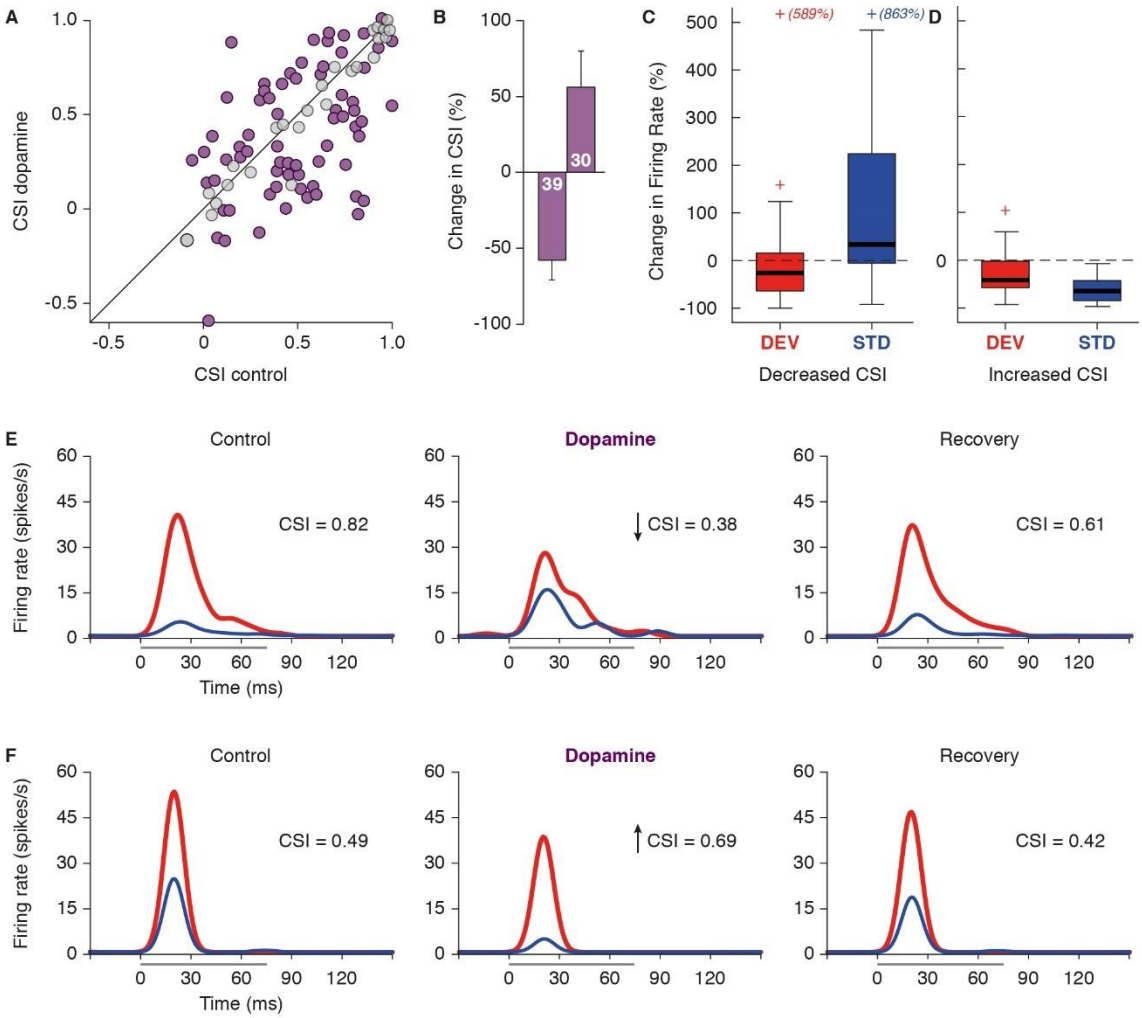

Figure 3. Effects of dopamine on the CSI. **A)** Scatter plot of the CSI in control condition versus dopamine application. Neurons that underwent significant CSI changes are represented in purple, whereas the rest are marked as grey dots. **B)** Average percent of change in the CSI for two groups of neurons: those where the CSI decreased and those where it increased significantly with dopamine application. **C)** Boxplots of the percent of change in the response to DEV and STD in the group of neurons where the CSI decreased. Data points between parenthesis represent outliers beyond scale. **D)** Boxplots of the percent of change in the response to DEV and STD in the group of neurons where the CSI increased. **E)** Example of the PSTH of a single unit before (left panel), during

(middle panel) and after (right panel) dopamine application. In this case, dopamine reduces the CSI. **F)** Another single unit example showing the opposite effects.

Figure 4

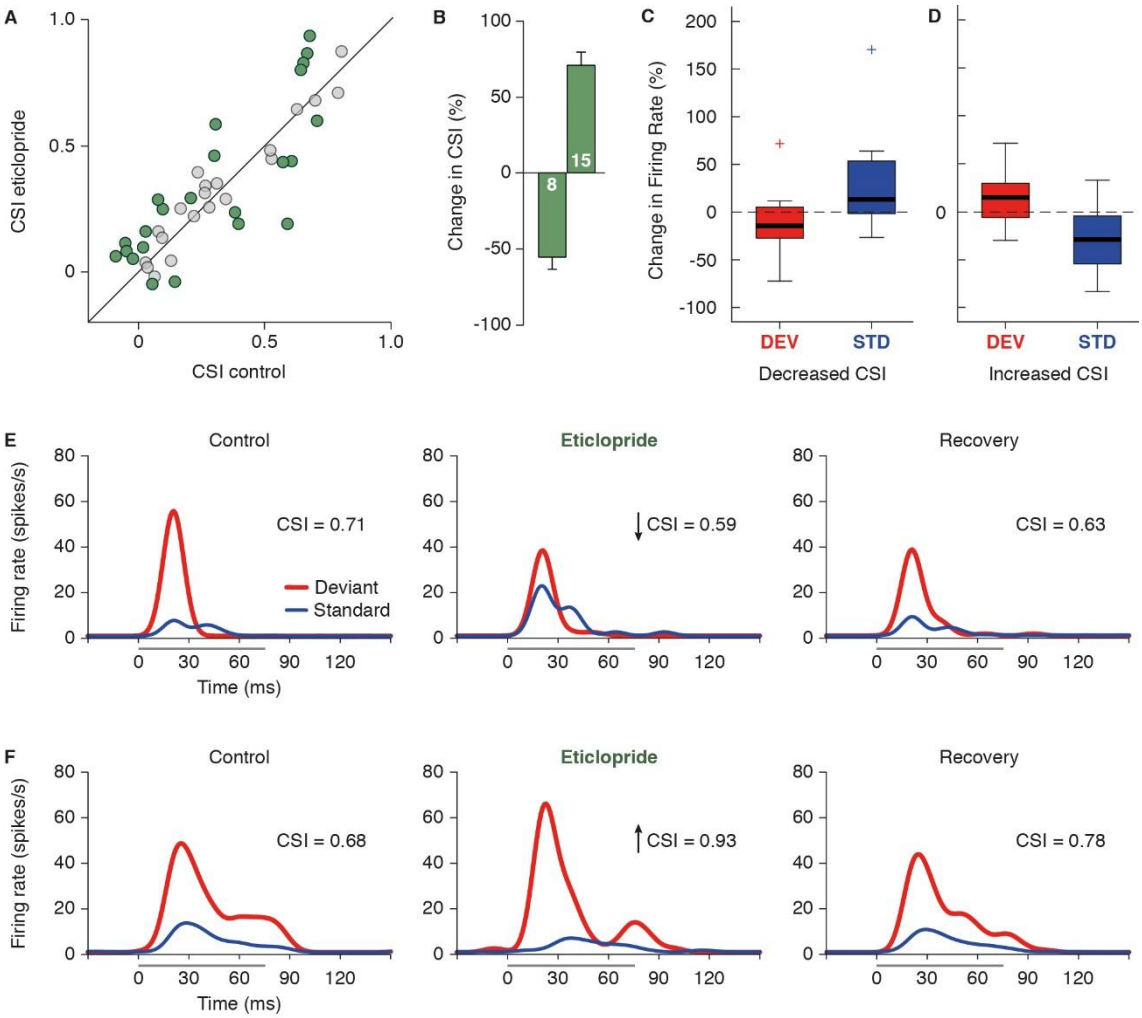

Figure 4. Effects of eticlopride on the CSI. **A)** Scatter plot of the CSI in control condition versus eticlopride application. Neurons that underwent significant CSI changes are represented in green, whereas the rest are marked as grey dots. **B)** Average percent of change in the CSI for two groups of neurons: those where the CSI decreased and those where it increased significantly with eticlopride application. **C)** Boxplots of the percent of change in the response to DEV and

STD in the group of neurons where the CSI decreased. **D)** Boxplots of the percent of change in the response to DEV and STD in the group of neurons where the CSI increased. **E)** Example of the PSTH of a single unit before (left panel), during (middle panel) and after (right panel) eticlopride application. In this case, eticlopride reduces the CSI. **F)** Another single unit example showing the opposite effects.

Figure 5

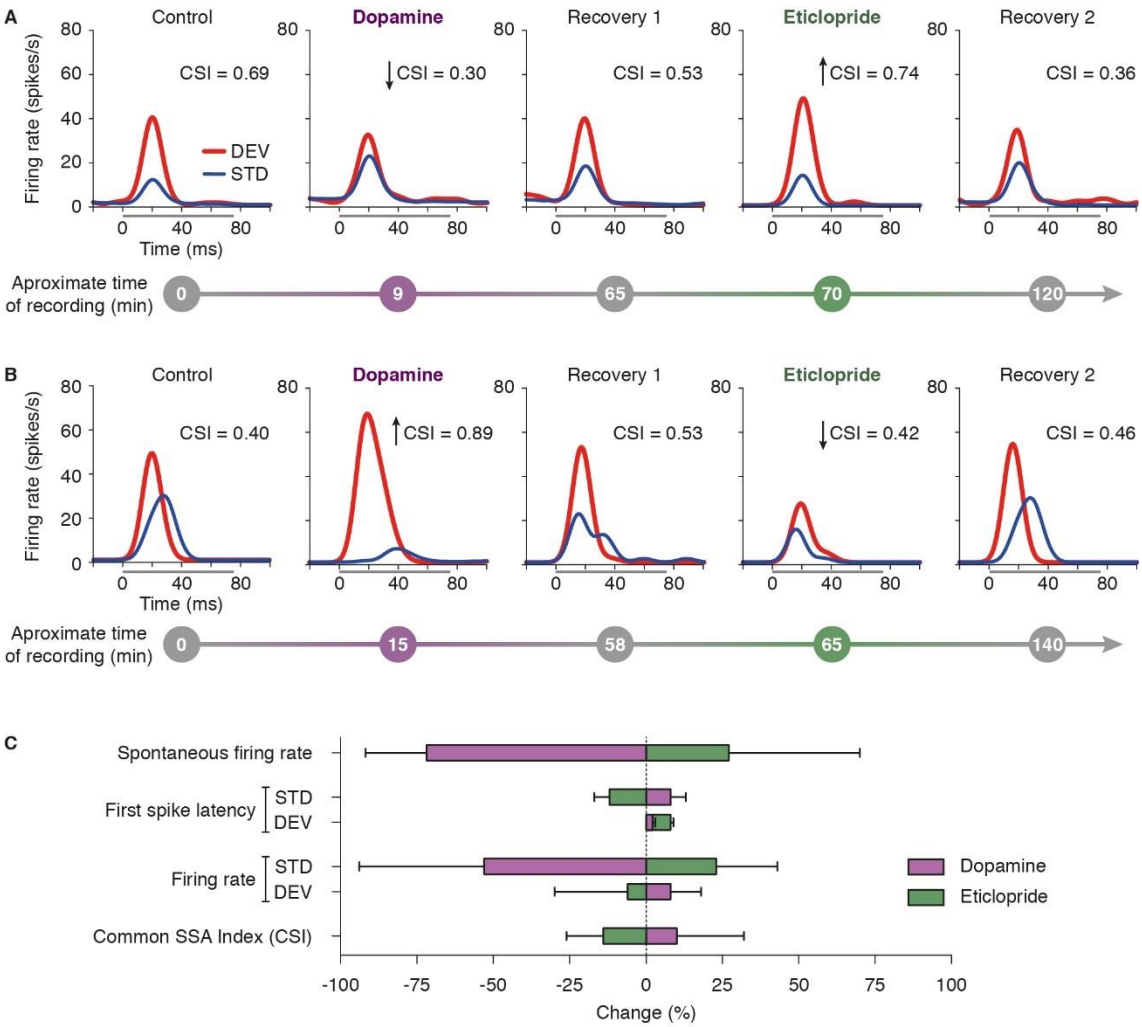

Figure 5. Antagonistic effects of dopamine and eticlopride application on the same neuron. **A)** Panels display the PSTH of a single unit under oddball stimulation. First panel on the left shows the neuronal response in the control

condition. The second panel shows a recording during dopamine application. The third panel shows a recording during the first recovery. The fourth panel shows a recording during eticlopride application. The last panel shows a recording during the second recovery. The diagram below the panels illustrates the temporal flow of the experiment. The colored circles indicate the approximate time relative to the first control recording when we observed the maximal effects of the drug or the recovery. The effect is a decrease of the CSI under dopamine influence and an increase under eticlopride. **B)** Panels display the PSTH of a neuron that showed the opposite effects. Dopamine application increased the CSI of this neuron, while eticlopride decreased the CSI. **C)** Bar plots represent the percent of change of spontaneous firing rate, first spike latency, firing rate and CSI caused by dopamine (purple bar) and eticlopride (green bar), denoting changes in opposite directions for the two drugs in most cases.

Figure 6

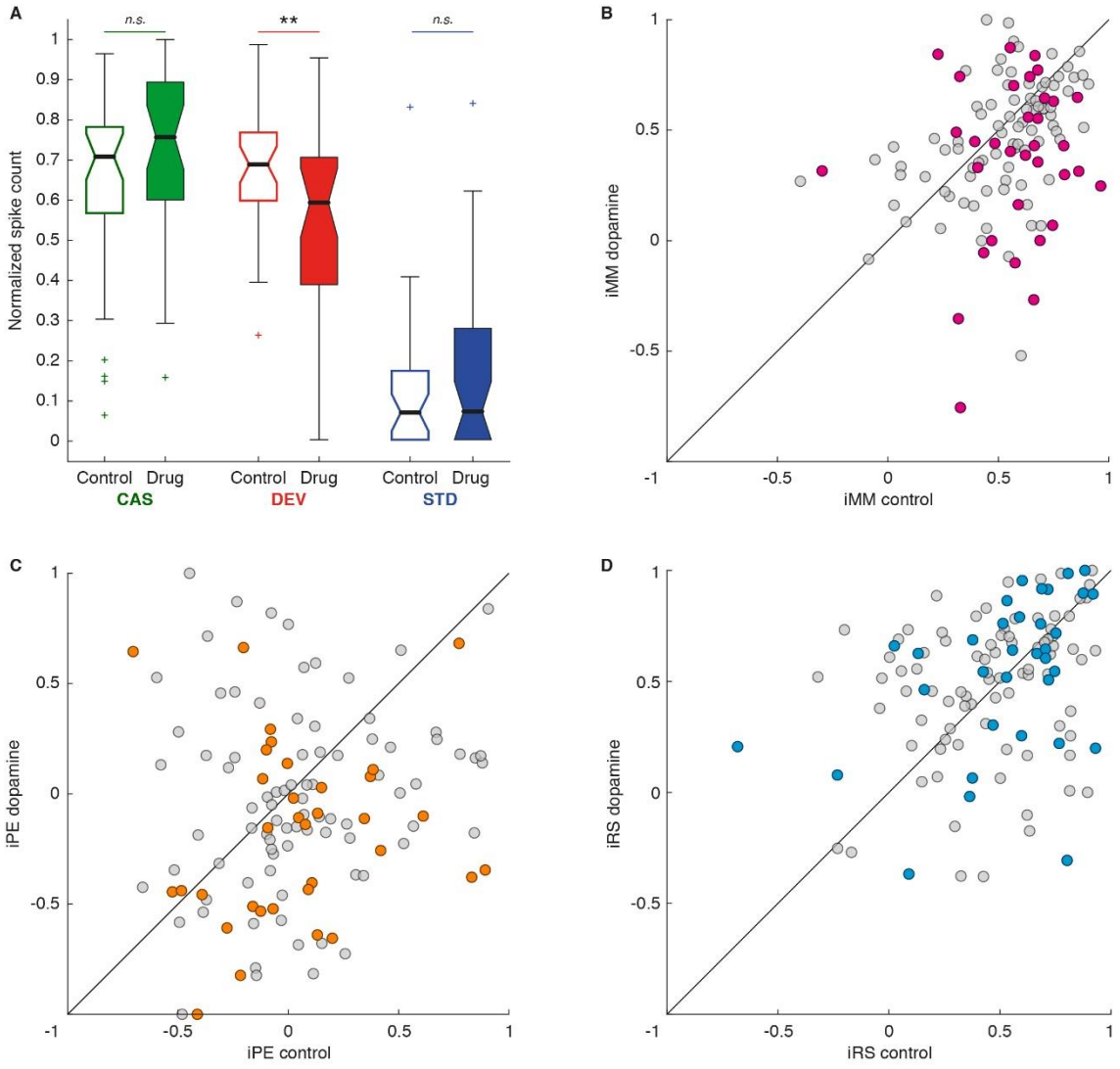

Figure 6. Effects of dopamine on the iMM, iPE and iRS. A) Notched boxplot showing the average normalized response to CAS, DEV and STD under control and dopamine conditions (n.s. indicates p>0.05; * indicates p<0.05; ** indicates p<0.01; *** indicates p<0.001). B) Scatter plot of the iMM in control condition versus dopamine application. Neurons that underwent significant iMM changes are represented in magenta, whereas the rest are marked as grey dots. C) Scatter plot of the iPE in control condition versus dopamine application. Neurons that underwent significant iMM changes are represented in orange, whereas the rest are marked as grey dots. D) Scatter plot of the iRS in control condition versus

dopamine application. Neurons that underwent significant iMM changes are represented in cyan, whereas the rest are marked as grey dots.

Figure 7

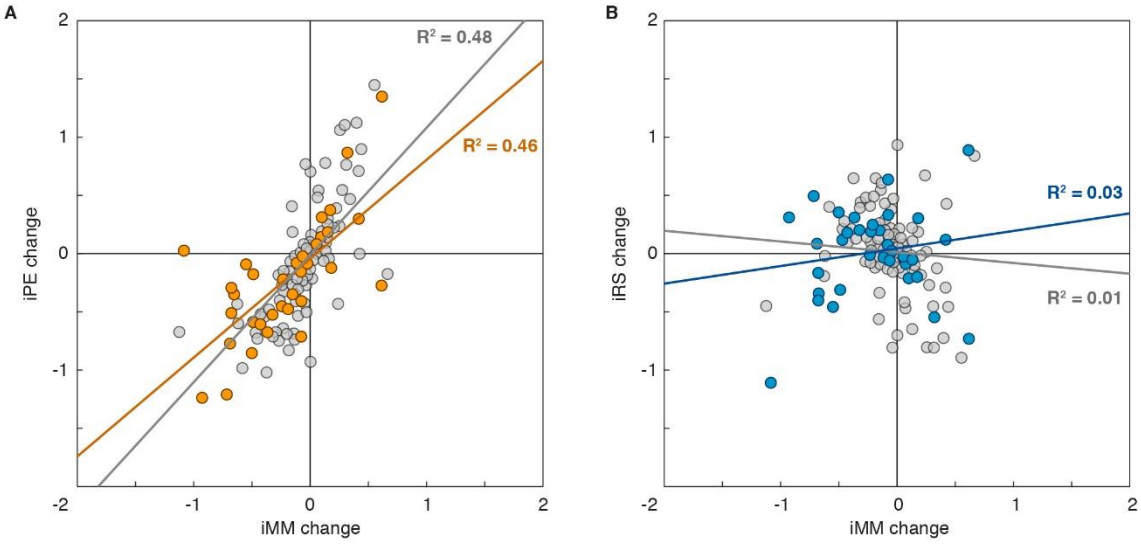

Figure 7. Relationship between the iMM changes with the dopaminergic modulation of the iPE and the iRS. **A)** Scatter plot representing iMM changes ($iMM_{dopamine} – iMM_{control}$) versus iPE changes ($iPE_{dopamine} – iPE_{control}$). Neurons that underwent significant iMM changes are represented in orange, whereas the rest are marked in grey. Linear regressions showed good fitness for the whole sample (orange and grey dots, gray line), as well as for the subpopulation that only included neurons that underwent significant iMM changes (orange dots only, orange line). **B)** Scatter plot representing iMM changes ($iMM_{dopamine} – iMM_{control}$) versus iRS changes ($iRS_{dopamine} – iRS_{control}$). Neurons that underwent significant iMM changes are represented in cyan, whereas the rest are marked in grey. Th linear regression model fit poorly, both for the whole sample (cyan and grey dots, gray line), and for the subpopulation that only included neurons that underwent significant iMM changes (cyan dots only, cyan line).

REFERENCES

1. Näätänen R, Gaillard AWK, Mäntysalo S. Early selective-attention effect on evoked potential reinterpreted. Acta Psychol (Amst). North-Holland; 1978;42: 313–329. doi:10.1016/0001-6918(78)90006-9

2. Ulanovsky N, Las L, Nelken I. Processing of low-probability sounds by cortical neurons. Nat Neurosci. 2003;6: 391–398. doi:10.1038/nn1032

3. Malmierca MS, Cristaudo S, Pérez-González D, Covey E. Stimulus-Specific Adaptation in the Inferior Colliculus of the Anesthetized Rat. J Neurosci. 2009;29: 5483–5493. doi:10.1523/JNEUROSCI.4153-08.2009

4. Malmierca MS, Carbajal GV, Escera C. Deviance Detection and Encoding Acoustic Regularity in the Auditory Midbrain. In: Kandler K, editor. The Oxford Handbook of the Auditory Brainstem. Oxford University Press; 2019. pp. 706–740. doi:10.1093/oxfordhb/9780190849061.013.19

5. Petersen CL, Hurley LM. Putting it in context: Linking auditory processing with social behavior circuits in the vertebrate brain. Integr Comp Biol. Oxford University Press; 2017;57: 865–877. doi:10.1093/icb/icx055

6. Ito T, Malmierca MS. Neurons, Connections, and Microcircuits of the Inferior Colliculus. In: Oliver D, Cant N, Fay R, Popper A, editors. The Mammalian Auditory Pathways. Springer, Cham; 2018. pp. 127–167. doi:10.1007/978-3-319-71798-2_6

7. Hurley LM. Neuromodulatory Feedback to the Inferior Colliculus. In: Kandler K, editor. The Oxford Handbook of the Auditory Brainstem. Oxford University Press; 2018.

doi:10.1093/oxfordhb/9780190849061.013.15

8. Hurd YL, Suzuki M, Sedvall GC. D1 and D2 dopamine receptor mRNA expression in whole hemisphere sections of the human brain. J Chem Neuroanat. Elsevier; 2001;22: 127–137. doi:10.1016/S0891-0618(01)00122-3

9. Nevue AA, Felix RA, Portfors C V. Dopaminergic projections of the subparafascicular thalamic nucleus to the auditory brainstem. Hear Res. 2016;341: 202–209. doi:10.1016/j.heares.2016.09.001

10. Gittelman JX, Perkel DJ, Portfors C V. Dopamine modulates auditory responses in the inferior colliculus in a heterogeneous manner. JARO - J Assoc Res Otolaryngol. 2013;14: 719–729. doi:10.1007/s10162-013-0405-0

11. Batton AD, Blaha CD, Bieber A, Lee KH, Boschen SL. Stimulation of the subparafascicular thalamic nucleus modulates dopamine release in the inferior colliculus of rats. Synapse. 2018: 0–2. doi:10.1002/syn.22073

12. Weiner DM, Levey AI, Sunahara RK, Niznik HB, O'Dowd BF, Seeman P, et al. D1 and D2 dopamine receptor mRNA in rat brain. Proc Natl Acad Sci U S A. National Academy of Sciences; 1991;88: 1859–63. doi:10.1073/PNAS.88.5.1859

13. Ayala YA, Malmierca MS. Cholinergic Modulation of Stimulus-Specific Adaptation in the Inferior Colliculus. J Neurosci. 2015;35: 12261–12272. doi:10.1523/JNEUROSCI.0909-15.2015

14. Valdés-Baizabal C, Parras GG, Ayala YA, Malmierca MS.

Endocannabinoid Modulation of Stimulus-Specific Adaptation in Inferior Colliculus Neurons of the Rat. Sci Rep. 2017;7: 6997. doi:10.1038/s41598-017-07460-w

15. Friston KJ. A theory of cortical responses. Philos Trans R Soc B Biol Sci. 2005;360: 815–836. doi:10.1098/rstb.2005.1622

16. Friston KJ. The free-energy principle: a rough guide to the brain? Trends Cogn Sci. 2009;13: 293–301. doi:10.1016/j.tics.2009.04.005

17. Garrido MI, Kilner JM, Stephan KE, Friston KJ. The mismatch negativity: a review of underlying mechanisms. Clin Neurophysiol. International Federation of Clinical Neurophysiology; 2009;120: 453–463. doi:10.1016/j.clinph.2008.11.029

18. Carbajal GV, Malmierca MS. The Neuronal Basis of Predictive Coding Along the Auditory Pathway: From the Subcortical Roots to Cortical Deviance Detection. Trends Hear. 2018;22: 233121651878482. doi:10.1177/2331216518784822

19. Ruhnau P, Herrmann B, Schröger E. Finding the right control: The mismatch negativity under investigation. Clin Neurophysiol. 2012;123: 507–512. doi:10.1016/j.clinph.2011.07.035

20. Wiens S, Szychowska M, Eklund R, van Berlekom E. Cascade and no-repetition rules are comparable controls for the auditory frequency mismatch negativity in oddball tasks. Psychophysiology. John Wiley & Sons, Ltd (10.1111); 2019;56: e13280. doi:10.1111/psyp.13280

21. Parras GG, Nieto-Diego J, Carbajal GV, Valdés-Baizabal C, Escera C,

Malmierca MS. Neurons along the auditory pathway exhibit a hierarchical organization of prediction error. Nat Commun. Springer US; 2017;8: 2148. doi:10.1038/s41467-017-02038-6

22. Parr T, Friston KJ. The Anatomy of Inference: Generative Models and Brain Structure. Front Comput Neurosci. Frontiers Media SA; 2018;12: 90. doi:10.3389/fncom.2018.00090

23. Parr T, Friston KJ. Uncertainty, epistemics and active Inference. J R Soc Interface. 2017;14. doi:10.1098/rsif.2017.0376

24. Bastos AM, Usrey WM, Adams RA, Mangun GR, Fries P, Friston KJ. Canonical Microcircuits for Predictive Coding. Neuron. 2012;76: 695–711. doi:10.1016/j.neuron.2012.10.038

25. Feldman H, Friston KJ. Attention, Uncertainty, and Free-Energy. Front Hum Neurosci. Frontiers; 2010;4: 215. doi:10.3389/fnhum.2010.00215

26. Friston KJ, Shiner T, FitzGerald THB, Galea JM, Adams RA, Brown HR, et al. Dopamine, affordance and active inference. Sporns O, editor. PLoS Comput Biol. Public Library of Science; 2012;8: e1002327. doi:10.1371/journal.pcbi.1002327

27. Hara K, Harris RA. The anesthetic mechanism of urethane: The effects on neurotransmitter-gated ion channels. Anesth Analg. Anesthesia and analgesia; 2002;94: 313–318. doi:10.1213/00000539-200202000-00015

28. Maggi CA, Meli A. Suitability of urethane anesthesia for physiopharmacological investigations in various systems. Part 1: General considerations. Experientia. 1986;42: 109–114. doi:10.1007/BF01952426

29. Sceniak MP, MacIver MB. Cellular Actions of Urethane on Rat Visual Cortical Neurons In Vitro. J Neurophysiol. American Physiological Society; 2006;95: 3865–3874. doi:10.1152/jn.01196.2005

30. Duque D, Malmierca MS. Stimulus-specific adaptation in the inferior colliculus of the mouse: anesthesia and spontaneous activity effects. Brain Struct Funct. Springer Berlin Heidelberg; 2015;220: 3385–3398. doi:10.1007/s00429-014-0862-1

31. Ayala YA, Pérez-González D, Duque D, Palmer AR, Malmierca MS. Extracellular Recording of Neuronal Activity Combined with Microiontophoretic Application of Neuroactive Substances in Awake Mice. J Vis Exp. 2016; e53914. doi:10.3791/53914

32. Pérez-González D, Hernández O, Covey E, Malmierca MS. GABA A-mediated inhibition modulates stimulus-specific adaptation in the inferior colliculus. Coleman MJ, editor. PLoS One. Erlbaum; 2012;7: e34297. doi:10.1371/journal.pone.0034297

33. Ayala YA, Malmierca MS. The effect of inhibition on stimulus-specific adaptation in the inferior colliculus. Brain Struct Funct. Springer Berlin Heidelberg; 2018;223: 1391–1407. doi:10.1007/s00429-017-1546-4

34. Paxinos G, Watson C. The rat brain in stereotaxic coordinates. Elsevier; 2007.

35. Nevue AA, Elde CJ, Perkel DJ, Portfors C V. Dopaminergic Input to the Inferior Colliculus in Mice. Front Neuroanat. 2016;9: 168. doi:10.3389/fnana.2015.00168

36. Hoyt JM, Perkel DJ, Portfors C V. Dopamine acts via D2-like receptors to modulate auditory responses in the inferior colliculus. eNeuro. Society for Neuroscience; 2019;6: ENEURO.0350-19.2019. doi:10.1523/ENEURO.0350-19.2019

37. LeBeau FE, Malmierca MS, Rees A. Iontophoresis in vivo demonstrates a key role for GABA(A) and glycinergic inhibition in shaping frequency response areas in the inferior colliculus of guinea pig. J Neurosci. Society for Neuroscience; 2001;21: 7303–12. doi:21/18/7303 [pii]

38. Malmierca MS. Chapter 29 – Auditory System. In: Paxinos G, editor. The Rat Nervous System. Academic Press; 2015. pp. 865–946. doi:10.1016/B978-0-12-374245-2.00029-2

39. Calabresi P, Mercuri NB, Sancesario G, Bernardi G. Electrophysiology of dopamine-denervated striatal neurons. Implications for Parkinson's disease. Brain. 1993;116 (Pt 2: 433–52. Available: http://www.ncbi.nlm.nih.gov/pubmed/8096420

40. Bamford NS, Robinson S, Palmiter RD, Joyce JA, Moore C, Meshul CK. Dopamine modulates release from corticostriatal terminals. J Neurosci. Society for Neuroscience; 2004;24: 9541–52. doi:10.1523/JNEUROSCI.2891-04.2004

41. Higley MJ, Sabatini BL. Competitive regulation of synaptic Ca2+ influx by D2 dopamine and A2A adenosine receptors. Nat Neurosci. NIH Public Access; 2010;13: 958–966. doi:10.1038/nn.2592

42. Michaeli A, Yaka R. Dopamine inhibits GABA(A) currents in ventral tegmental area dopamine neurons via activation of presynaptic G-protein

coupled inwardly-rectifying potassium channels. Neuroscience. 2010;165: 1159–69. doi:10.1016/j.neuroscience.2009.11.045

43. Moran RJ, Campo P, Symmonds M, Stephan KE, Dolan RJ, Friston KJ. Free Energy, Precision and Learning: The Role of Cholinergic Neuromodulation. J Neurosci. 2013;33: 8227–8236. doi:10.1523/JNEUROSCI.4255-12.2013

44. Friston KJ, Schwartenbeck P, FitzGerald THB, Moutoussis M, Behrens T, Dolan RJ. The anatomy of choice: Dopamine and decision-making. Philos Trans R Soc B Biol Sci. The Royal Society; 2014;369. doi:10.1098/rstb.2013.0481

45. Schultz W. Dopamine reward prediction error coding. Dialogues Clin Neurosci. Nature Publishing Group; 2016;18: 23–32. doi:10.1038/nrn.2015.26

46. Fiorillo CD, Tobler PN, Schultz W. Discrete coding of reward probability and uncertainty by dopamine neurons. Science (80-). 2003;299: 1898–1902. doi:10.1126/science.1077349

47. Schultz W, Dickinson A. Neuronal Coding of Prediction Errors. Annu Rev Neurosci. Annual Reviews 4139 El Camino Way, P.O. Box 10139, Palo Alto, CA 94303-0139, USA; 2000;23: 473–500. doi:10.1146/annurev.neuro.23.1.473

48. Yasui Y, Nakano K, Mizuno N. Descending projections from the subparafascicular thalamic nucleus to the lower brain stem in the rat. Exp Brain Res. 1992;90: 508–518. doi:10.1007/BF00230933

49. LeDoux JE, Ruggiero DA, Reis DJ. Projections to the subcortical forebrain from anatomically defined regions of the medial geniculate body in the rat. J Comp Neurol. Wiley-Blackwell; 1985;242: 182–213. doi:10.1002/cne.902420204

50. Yasui Y, Kayahara T, Nakano K, Mizuno N. The subparafascicular thalamic nucleus of the rat receives projection fibers from the inferior colliculus and auditory cortex. Brain Res. 1990;537: 323–327. doi:10.1016/0006-8993(90)90378-O

51. Wang J, Palkovits M, Usdin TB, Dobolyi A. Afferent connections of the subparafascicular area in rat. Neuroscience. 2006;138: 197–220. doi:10.1016/j.neuroscience.2005.11.010

52. Arnault P, Roger M. Ventral temporal cortex in the rat: Connections of secondary auditory areas Te2 and Te3. J Comp Neurol. Wiley-Blackwell; 1990;302: 110–123. doi:10.1002/cne.903020109